J Mater Sci: Mater Med (2010) 21:2955–2969
DOI 10.1007/s10856-010-4127-0

Development of porous HAp and β-TCP scaffolds by starch consolidation with foaming method and drug-chitosan bilayered scaffold based drug delivery system

B. Kundu · A. Lemos · C. Soundrapandian · P. S. Sen · S. Datta · J. M. F. Ferreira · D. Basu

Received: 7 March 2010 / Accepted: 2 July 2010 / Published online: 20 July 2010

Abstract The inability to maintain high concentrations of antibiotic at the site of infection for an extended period of time along with dead space management is still the driving challenge in treatment of osteomyelitis. Porous bioactive ceramics such as hydroxyapatite (HAp) and beta-tri calcium phosphate (β-TCP) were some of the alternatives to be used as local drug delivery system. However, high porosity and high interconnectivity of pores in the scaffolds play a pivotal role in the drug release and bone resorption. Ceftriaxone is a cephalosporin that has lost its clinical popularity. But has recently been reported to exhibit better bactericidal activity in vitro and reduced probability of resistance development, in combination with sulbactam, a β-lactamase inhibitor. In this article, a novel approach of forming HAp and pure β-TCP based porous scaffolds by applying together starch consolidation with foaming method was used. For the purpose, pure HAp and β-TCP were prepared in the laboratory and after thorough characterization (including XRD, FTIR, particle size distribution, etc.) the powders were used for scaffold fabrication. The ability of these scaffolds to release drugs suitably for osteomyelitis was studied in vitro. The results of the study indicated that HAp exhibited better drug release profile than β-TCP when drug was used alone indicating the high influence of the carrier material. However, this restriction got relaxed when a bilayered scaffold was formed using chitosan along with the drug. SEM studies along with EDAX on the drug-chitosan bilayered scaffold showed closest apposition of this combination to the calcium phosphate surface.

B. Kundu (✉) · C. Soundrapandian · P. S. Sen · S. Datta · D. Basu
Bioceramics and Coating Division, Central Glass and Ceramic Research Institute, Kolkata 700032, India
e-mail: biswa_kundu@rediffmail.com

C. Soundrapandian
e-mail: soundr@rediffmail.com

P. S. Sen
e-mail: pssen@cgcri.res.in

S. Datta
e-mail: sdatta@cgcri.res.in

D. Basu
e-mail: dbasu@cgcri.res.in

A. Lemos · J. M. F. Ferreira
Department of Ceramics and Glass Engineering, CICECO, University of Aveiro, Aveiro 3810193, Portugal
e-mail: alemos@ua.pt

J. M. F. Ferreira
e-mail: jmf@ua.pt

1 Introduction

The inability to maintain high concentrations of antibiotic at the site of infection for an extended period of time is considered as the major reason for failures in osteomyelitis treatment [1, 2]. Rational approach for osteomyelitis treatment often combines local delivery of antimicrobials following surgery. Though local delivery offers several advantages including higher concentrations of drugs available at the target site with reduced adverse effects; the surgical procedure resulting in bone defect persists as a problem [3]. Implant material, viz. antibiotic-impregnated acrylic bone cement beads has shown various problems like requirement for removal of the beads at the later stages, thermal damage to some antibiotics, poor and

incomplete drug elution and persistence of bacterial growth on the implant itself [4–6].

Porous Hydroxyapatite (HAp) and/or Beta-tri calcium phosphate (β-TCP) have been widely used as a bone substitute materials having drug delivery ability because of their excellent biocompatibility, osteoconductive and osteoinductive properties [7–12]. Ideally, HAp used for sustained release of drug to bone should have both large pores ($\sim$100 μm) to allow bone ingrowth into the pores of HAp and small pores to facilitate the slow release of drug [13]. Bioactive materials with open porosity and pore diameters greater than $\sim$100 μm can allow bioactive fixation, with direct attachment by chemical bonding with the bone [14–16]. There are some general problems exist in controlling the parameters to obtain porous ceramics with desired pore structure and component dimensions [17]. Recently "starch consolidation", that uses starch granules as pore formers and consolidator agent has been introduced that gives good homogeneity of the consolidated bodies [18, 19]).

Various classes of antibiotics as cephalosporins, fluoroquinolones, β-lactams, glycopeptides etc., have been studied for their effectiveness against osteomyelitis. It has been reported that cephalosporins is not appreciably effective in osteomyelitis due to the β-lactamase production of the main causative agent, *Staphylococcus aureus*. Ceftriaxone is a cephalosporin that has lost its clinical popularity. But has recently been reported to exhibit better bactericidal activity in vitro and reduced probability of resistance development, in combination with sulbactam, a β-lactamase inhibitor [20]. Therefore it has been assumed that this combination in the treatment of orthopedic infections or in the development of local drug delivery may be ideal to establish their respective effectiveness. On the other hand, chitosan, a biocompatible polysaccharide composed of glucosamine and N-acetyl glucosamine linked with β 1–4 glucosidic linkage, has been studied in many biomedical fields, including tissue engineering for bone, blood vessel and nerve [21–23]. In order to improve the bioactivity of chitosan in bone tissue engineering and get mouldable HAp-contained materials, i.e. for osteochondral approach, chitosan/nano-HAp composite/bi-layered scaffolds have been reported [24]. Nevertheless, its efficacy for sustained release of drugs has not thoroughly been studied.

In the present investigation, therefore, a systemic attempt has been made to fabricate highly interconnected HAp and β-TCP based porous scaffold for drug delivery by applying together starch consolidation and foaming method. A bilayered coating was also provided to the pore surfaces of some samples using chitosan and β-lactamase–cephalosporin derivative to assess their effect on sustained drug releasing.

2 Materials and methods

2.1 Synthesis of different calcium phosphate powders

Pure hydroxyapatite and β-TCP were synthesized in the laboratory by following a simple wet chemical method using analytical reagent grade calcium hydroxide [$Ca(OH)_2$] (Central Drug House, India) and ortho-phosphoric acid (H_3PO_4) (Ranbaxy Lab. Ltd., India) for HAp and calcium carbonate ($CaCO_3$) (Sigma–Aldrich, USA) and H_3PO_4 for β-TCP as the sources of calcium and phosphorous for the powders respectively. Initial raw materials were mixed in order maintain the Ca/P ratios of about 1.67 and 1.50 for HAp and β-TCP respectively which should produce stoichiometric HAp and β-TCP after calcination at 1000 °C. The details of the process have been published elsewhere [25, 26]. The filtered cake thus obtained was first dried in an air oven for 24 h at 100 °C, ground and characterized. Calcinations were carried out 1000 °C for both the powders which were used subsequently for fabrication of porous scaffolds. Some powder samples were fired at 1200 and 1250 °C for HAp and β-TCP respectively for assessment of phases.

2.2 Powder characterization

2.2.1 X ray diffraction (XRD) and Fourier transformed infra-red spectroscopy (FTIR)

The phase composition, degree of crystallinity, crystallite size, etc. of the powders calcined at different temperatures were analyzed by XRD (Philips Analytical B.V., X'Pert Pro, Netherlands) powder diffractometer. Continuous data were collected over the 2θ range 20–60°, using monochromatic Cu $K_{\alpha 1}$ radiation (operating conditions being 30 mA and 40 kV and wavelength of 1.5406 Å), with a step size of 0.017° and a count time of 10.34 s. The diffraction patterns were compared with the database of Joint Committee on Powder Diffraction Standards Powder Diffraction Files (JCPDS PDFs). FTIR was used to ascertain the functional groups present and stereochemistry of the powders calcined at different temperatures. The alkali halide disk technique was employed and middle-IR spectra (4000–400 cm^{-1}) were obtained with a double beam spectrophotometer (Spectrum 100, Perkin-Elmer, USA) with $\pm$ 2 cm^{-1} resolution.

2.2.2 Particle size distribution (PSD) and specific surface area (SSA) by BET method

Calcined powders (1000 °C) were planetary milled (PM400, Retsch, Gernmany) in a zirconia container in propanol medium for 4 h to reduce particle size and

increase of surface area. The powders before and after milling were suspended in ultra-pure water obtained from Milli-Q system (Milli-Q Academic Century, ZMQS50001, China) (0.20 g in 20 c.c.) by using a high intensity ultrasonic probe (Electronic Industries, India) operated at 20 kHz with power 100 W for 4 h and subsequently particle size distribution was measured by a particle size analyzer (Micromeritics Sedigraph 5100, USA. Specific surface area (SSA, and average particle size calculated from these values) of the powders (S_{BET}) was measured using multi point BET method (Micromeritics ASAP2010, USA).

2.2.3 *Surface charge analysis*

Surface charge in terms of zeta potential of the powder (calcined powders fired at 1000°) suspensions were estimated for optimization of the slurries/suspensions for direct consolidation casting and assessing the interaction between these particles and drug/chitosan. Zeta potential of different calcium phosphate particles were determined with a Coulter Delsa 440 SX, USA using suspensions containing 0.01 wt% of different particles in a 10^{-3} M KCl solution. The measurements were taken as a function of pH at 20 °C. The pH was adjusted with 0.1 M KOH and 1 M HCl solutions for basic and acidic conditions respectively.

2.3 Fabrication of porous scaffolds

2.3.1 *Slip preparation*

Anionic dispersant (Dispex N40, Ciba Specialty Chemicals Inc. U.K.) was used to deflocculate both HAp and β-TCP suspensions and this was chosen based on a pilot study with the effect of dispersant on electrophoretic, sedimentation and viscosity properties, the description of which has been published elsewhere [27, 28]. During the optimization of deflocculation of the suspension, pH was varied using aqueous solutions of 1 M HCl and 0.1 M KOH. Rheological property measurements of each slip batch through zeta potential and viscosity indicated that 45 vol% solid loading with 0.8–1.2 wt% of dispersant was required for optimum deflocculation and sufficient flow ability for HAp and β-TCP and this slurry was used subsequently for fabrication of porous body.

2.3.2 *Porous sample preparation and characterization*

Etherified potato starch modified by hydroxyl-propylation and cross linking (TRECOMEX AET1, Lyckeby Starkelsen AB, Sweden) of 10 vol% of solid content was added to the stock suspension (45 vol%) prior to the incorporation of the foaming agents to act as pore former and binder of the green body. On heating the suspension in the range 55–80 °C, the starch granules start to absorb water from the surroundings, undergoing a rapid and irreversible swelling [19].

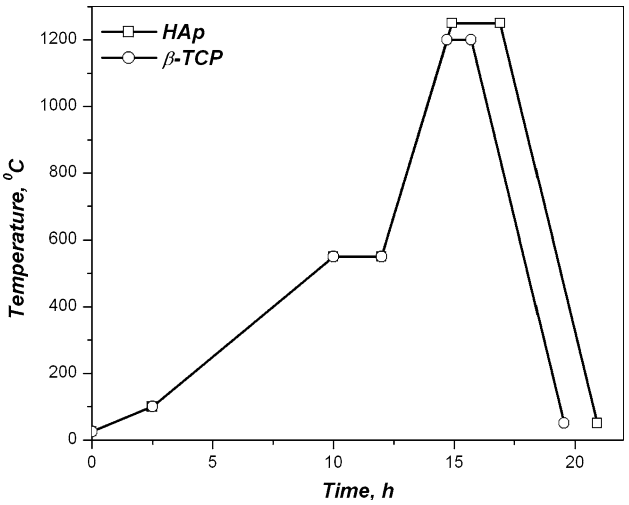

Fig. 1 Heating schedule for sintering of HAp and β-TCP porous scaffold

Combination of foaming agents like foam-bath concentrate (FBC; Dibel, S. A., Porto, Portugal) and Sodium Lauril Sulphate (SLS; Texapon k12, V.P., Lisbon, Portugal) were added to the slip in different weight fractions. The slurries were homogenized through mechanical stirring and finally poured into a closed silicon mould, consolidated at 80 °C for 1 h, de-moulded and dried at 60 °C for 24 h, and further at 110 °C for 24 h. The dried samples were sintered according to the heating schedule, given in Fig. 1.

Physical properties of the porous blocks like percentage of porosity, bulk density of the sintered samples were determined using Archimedes' water displacement method while microstructure and pore morphology was observed by scanning electron microscopy (SEM; Leo 430i Stereoscan, U.K.). The samples were mounted and sputter-coated with gold–palladium having a coating thickness ~6 nm to reduce charging and to improve the image quality prior testing. Compressive strength of the samples (with length:diameter ~2:1) were also measured by an Instron (UTM 5500R, Instron, USA) following ASTM C773 standard [29] with a crosshead speed of 1 mm/min.

2.4 Preparation of drug delivery system

In the present investigation, porous HAp and TCP samples having 10 mm dia. × 10 mm length were infiltrated with a combination of antibiotic drugs (ceftriaxone sodium and sulbactum sodium in 2:1 w/w ratio, hereinafter the composite drug would be designated as CFS). In a 500 mg/ml

Table 1 Sample details and designation

Name	Details
Gr. I	Only-drug loaded HAp sample
Gr. II	Only-drug loaded TCP sample
Gr. III	Bi-layered (drug and chitosan) HAp sample
Gr. IV	Bi-layered (drug and chitosan) TCP sample

concentrated solution of said drugs, porous bioceramic scaffolds were soaked and vacuum infiltrated under high vacuum (10^{-3} Torr) for of 1 h and subsequently freeze dried at a temperature of −80 °C for 4 h. The amount of drug loaded was calculated from the weight gain of the respective samples. A 0.5 wt% chitosan solution was prepared by dissolving chitosan of medium molecular weight (Aldrich, USA) and a degree of deacetylation of ~85% in 0.2 M acetic acid solution. Some of the drug loaded porous scaffolds of both HAp and β-TCP were once again taken into cylindrical silicon moulds in which chitosan solution was also added. The impregnation was ensured after placing the silicone mould again under high vacuum for prolonged time and freeze-drying at −80 °C up to 2 days to completely remove the frozen solvent. The chitosan was not cross-linked using some cross linker in this study. The samples were then divided into 4 groups and henceforth would be designated as Gr. I–IV, the details of which are given in Table 1.

2.4.1 SEM and EDAX analysis

A section of these bi-layered (drug and chitosan) porous blocks was further characterized for microstructural evolution using SEM (Leo 430i Steroscan, U.K.). Depending on the samples' composition, microstructures were taken either in secondary electron or back-scatter electron mode. For assessment of the compositional variation along the interface energy-dispersive analysis of X ray (EDAX) was employed (spot size: 520 nm, SiLi detector and collection time: 45 s). Depending on the microstructure observed, either line-scan or area-scan of EDAX of the surface was performed. Carbon sputter coating of ~15–20 nm thickness was given prior such observation of SEM–EDAX.

2.4.2 Drug release study

Ceftriaxone sodium and sulbactum sodium release tests from different porous ceramic matrices (for all groups i.e. Gr. I to IV) were performed at 37 ± 2 °C in phosphate buffer saline (PBS) at pH 7.4. Each drug loaded porous sample was immersed in 50 ml of dissolution medium in a polyethylene bottle. Aliquots (2 ml) of the 50 ml PBS were withdrawn at regular intervals (daily basis from day 1 to day 7 and subsequently with a gap of 7 days) up to 42 days from each flask and replaced with fresh phosphate buffer. The drugs have been quantitatively determined in the soup by means of a UV–Vis Spectrophotometer (Lambda 25, Perkin–Elmer, USA). The absorbance has been measured at a fixed wavelength: 240 and 270 nm (each data point is the mean of three values) characteristics of the above combined drugs. The spectrophotometer was calibrated prior using for estimation of eluted drug.

Meanwhile, the effect of chitosan on release profile from this composite drug has also been checked using the same UV–Vis spectrophotometer. Different amounts of chitosan (0.25–1 wt%) were added to a constant concentration of drug (5 μg/mL) and subsequently checked through UV–Vis at the same fixed wavelength: 240 and 270 nm.

3 Results and discussion

3.1 Powder characterization

X ray diffraction of the powders prepared at 80 °C together with the powders fired at 1000 °C and 1250 are given in Figs. 2 and 3. XRD was carried out to show the changes of different crystalline parameters including percentage of phase, percentage of crystallinity and average crystallite size, etc. during the course of this heat treatment. The respective positions of the XRD peaks were compared with Joint Committee on Powder Diffraction Standards, Swarthmore, PA, USA (JCPDS) standard powder diffractions files (PDFs). XRD data analysis showed that in case of powder synthesized using calcium hydroxide and orthophosphoric acid as the starting materials and the same powder fired at different temperatures were primarily composed of single phase of hydroxyapatite, which was matched with PDF no. 09-0432 (Fig. 2a–c).

The as-dried powder intended to synthesize pure β-TCP, was primarily composed of calcium hydroxide phosphate and matched with PDF no. 74-0566, which was subsequently converted to pure β-TCP (matched with PDF no. 09-0169) when calcined at 1000 °C and thereafter at 1200, calcium pyrophosphate (α-$Ca_2P_2O_7$) (matched with PDF no. 09-0345). Quantitative percent phase/s present was calculated by internal standard method of XRD [30]. Required mass absorption coefficient values for β-TCP, α-$Ca_2P_2O_7$ and mixtures of these two phases were taken as 95.5864, 76.9949 and 81.8298 respectively. Average crystallite size and degree of crystallinity of as-prepared and calcined powders were estimated from the relationships derived by Scherer [31] and Landi et al [32] and results are summarized in Fig. 4. For samples containing an amorphous fraction, the percent crystallinity was determined as the sum of all the weight fractions of the

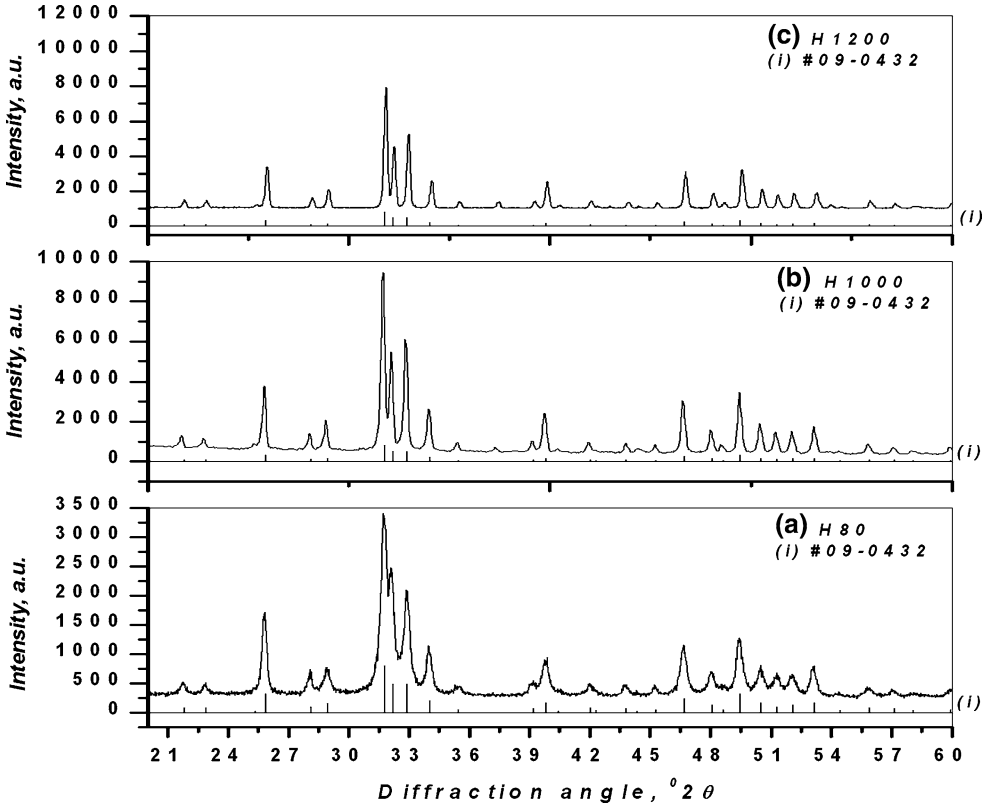

Fig. 2 XRD of the powders for HAp. **a** As-prepared (H80), **b** calcined at 1000 °C (H1000) and **c** calcined at 1250 °C (H1250); (*i*) is the corresponding JCPDS PDF

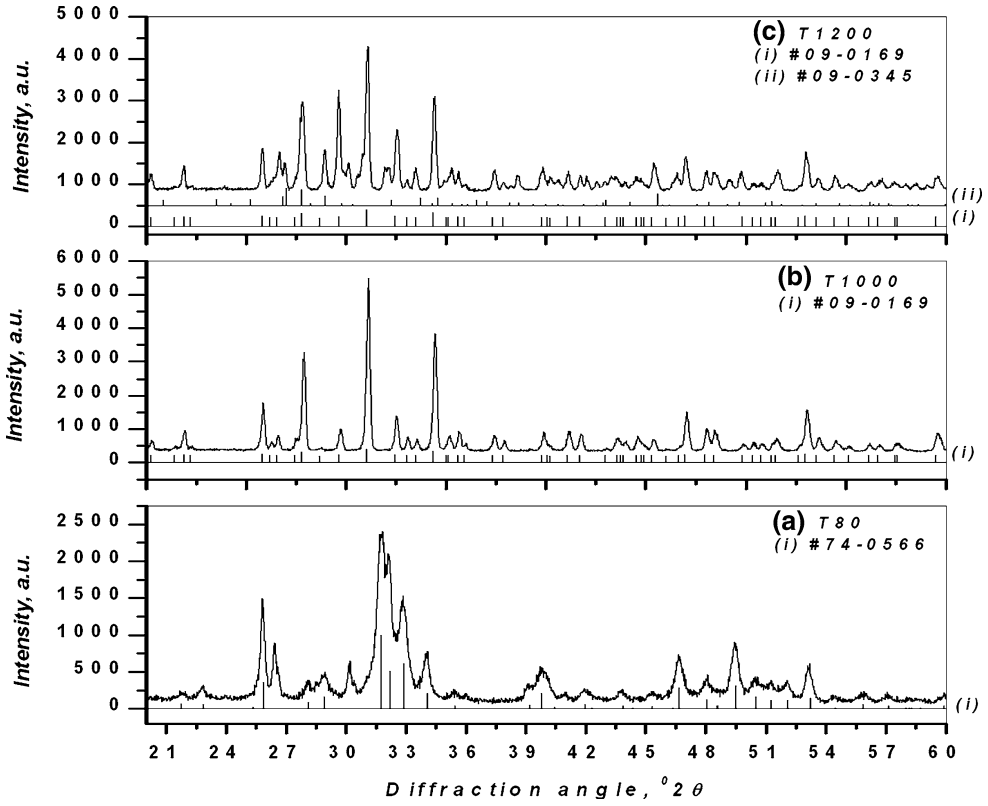

Fig. 3 XRD of the powders for β-TCP. **a** As-prepared (T80), **b** calcined at 1000 °C (T1000) and **c** calcined at 1200 °C (T1200); (*i*) and (*ii*) are the corresponding JCPDS PDFs

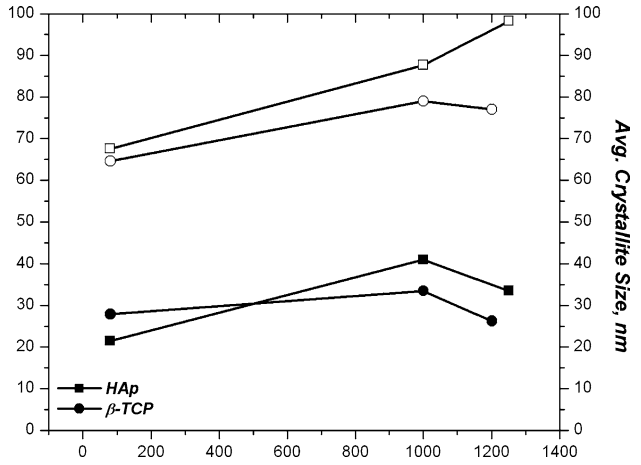

Fig. 4 Variation of percent of crystallinity and average crystallite size with temperature as calculated from the XRD patterns given in Figs. 2 and 3

crystalline phases in the mixture, which will be less than unity. Degree of crystallinity of composite phase obtained for the TCP powders fired at 1200 °C was calculated by taking the ratio of peak for coherent scattering to background (i.e. incoherent scattering) w.r.t. the standard material for β-TCP [33].

Degree of crystallinity was less in case of β-TCP than HAp at a particular temperature. This parameter has an effect for attachment of drug and/or chitosan and subsequently its elution in physiological fluid. It is generally expected that more the amorphous content (i.e. low degree of crystallinity) in a particular material more would be said organic attachment to the crystals of both HAp and β-TCP. Lower degree of crystallinity for TCP was due to probable dissociation of β-TCP to α-calcium pyrophosphate at higher temperature. Percentage of the secondary phase for TCP was calculated and found to be about 12% with $\sim$23% amorphous phase. Crystallinity degree of the starting powders directly influences the densification behaviour and kinetics. As the crystallinity degree of the starting powder decreases, activation energy for grain boundary diffusion is lowered; in fact, the grain boundary moves with the aim of reducing its total extension influencing grain growth rate [32].

Figures 5 and 6 show the FTIR spectrum of the powders calcined at different temperatures for both HAp and β-TCP respectively. The band assignments for the spectrum obtained at these different temperatures could be summarized in Table 2. Very small hump at the wavenumbers 1454 and 1414 cm^{-1} arose from vibrations of CO_3^{2-} ions in Fig. 5a and b. The presence of carbon modes in the samples indicates the presence of impurity in these samples coming from the raw materials or the atmosphere during the preparation process which was not detected in the XRD pattern [34]. The peak almost disappeared upon firing at 1250 °C. In every spectrum there was a circle marked around 2362 cm^{-1} which came from the atmosphere and hence ignored for subsequent interpretation processes. In case of β-TCP, the band at 1416 cm^{-1} showing presence of CO_3 group which was introduced during the process of reaction. As-dried powder had some carbonate ions with a calcium deficient calcium phosphate phase. This defective calcium phosphate was converted into HAp or β-TCP depending on the thermal condition and atmosphere of firing. Again, HAp tends to transform into β-TCP on

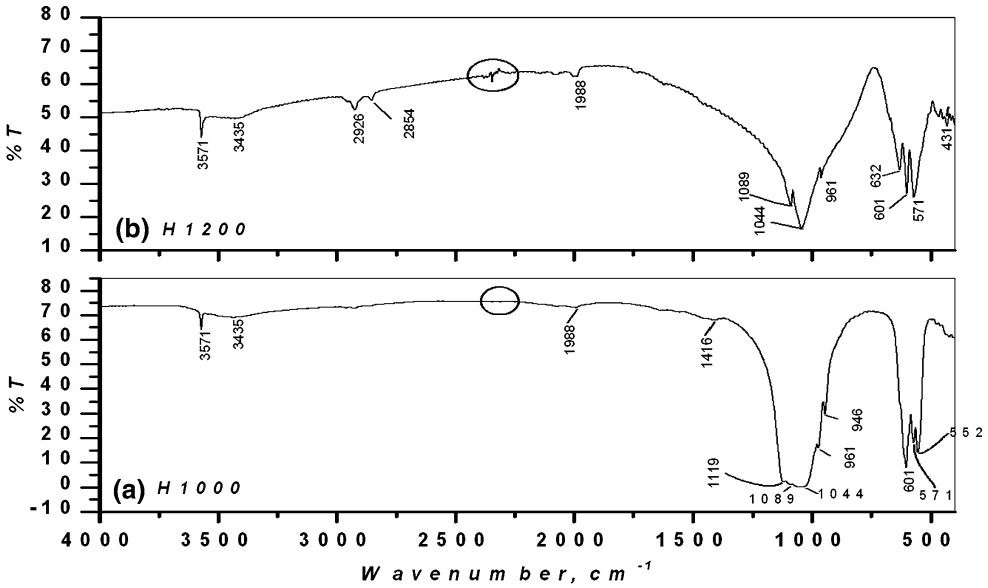

Fig. 5 FTIR of the powders for HAp. **a** calcined at 1000 °C (H1000) and **b** calcined at 1250 °C (H1250); *Circle mark* corresponds atmosphere CO_2

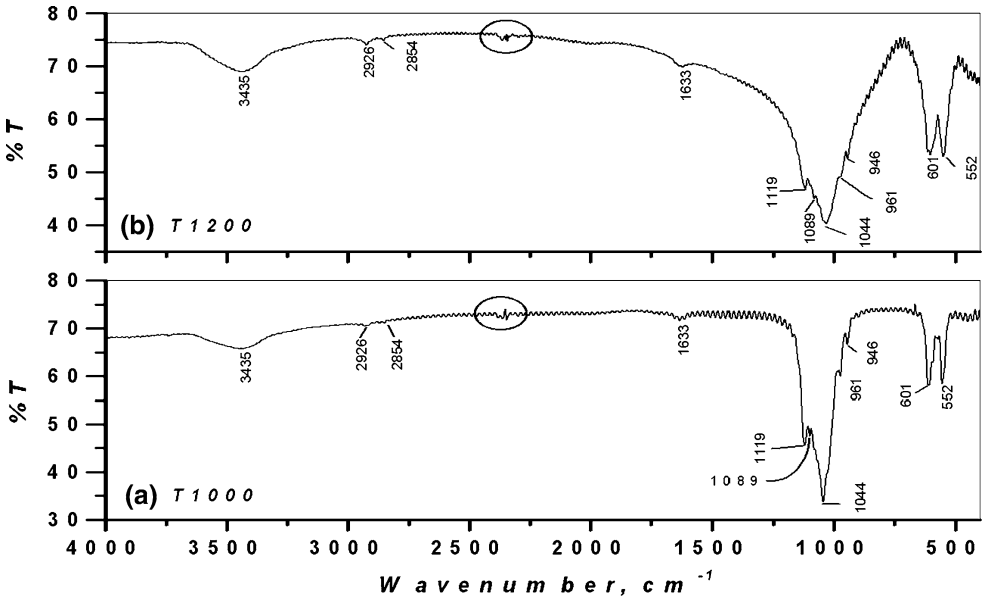

Fig. 6 FTIR of the powders for β-TCP. **a** calcined at 1000 °C (T1000) and **c** calcined at 1200° C (T1200); *Circle mark* corresponds atmosphere CO_2

Table 2 Band assignments of FTIR spectrum given in Figs. 5 and 6

Wavenumber, cm^{-1}	Assignment/s
3700–3000	H–O–H, Water of crystallization or adsorbed water
3580	O–H, (OH) group
1615	H–O–H, Water of crystallization or adsorbed water
1454, 1414	C–O of CO_3 groups
1119, 1098	P–O and P–OH, HPO_4, and PO_4 groups
1030	P–O in HPO_4, and PO_4 groups (stretching mode)
965	P–O in PO_4 group
865	P–OH stretching mode of HPO_4 groups
630	O–H of OH group
600, 564	P–O in PO_4 groups (bending mode)
525	HO–PO_3 bending mode in HPO_4

heating at 900 °C depending on the deficiency of calcium and based on the following reaction [35, 36]:

$$Ca_{10-x}(HPO_4)_x(PO_4)_{6-x}(OH)_{2-x} \rightarrow (1-x)Ca_{10}(PO_4)_6(OH)_2 + 3x\beta - Ca_3(PO_4)_2 + xH_2O$$

where, x is the calcium deficiency. Carbonate content in the powder was disappeared as seen from Fig. 6a. Phosphate ions have four vibration modes viz. ν_1, ν_2, ν_3 and ν_4 [37]. The observed bands at 965 are ν_2 modes of phosphate ion, transmission bands corresponding ν_3 phosphate ion (1119 and 1044 cm^{-1}) are also distinguishable from Fig. 6a. Bands at 601 cm^{-1} corresponded ν_4 mode of phosphate ion [37, 38]. Band positions like 2926 and 2854 cm^{-1} resembled presence of OH functional group, which was not incorporated into the crystal structure [39]. As before, in every spectrum there was a circle marked around 2362 cm^{-1} which came from the atmosphere and hence ignored for subsequent interpretation. Phosphate ion band characteristic for β-TCP at 945 cm^{-1} was also evident.

3.2 Characterization of slip and porous microstructure

Parameters such as the size, size distribution, and shape of the particles influence the compressibility and, hence, the packing density of the cast [40]. Since particles with less than 10 μm size with a proper distribution produces casts with a higher packing density, calcined (1000 °C) HAp powder that had a bimodal size distribution was planetary milled to obtain a well-distributed suspension with median particle size ~3.5 μm (Fig. 7a). The TCP powder (similarly calcined at 1000 °C) exhibiting a multi-modal particles size distribution was planetary ball milled to obtain a well-distributed one with median particles size ~2.9 μm (Fig. 7b). Particle sizes calculated from specific surface area also confirmed the above results. The specific surface areas obtained from BET plots were found to be ~0.5 and 0.64 m^2/g for HAp and TCP powders with corresponding particle sizes of 3.8 and 3.04 μm respectively.

To avoid excessive shrinkage during densification slurries containing high volume fraction of particles is desirable. Accordingly, slurries with a 45 vol% solids were used in the present investigation. For casting porous layers, the same slurry with added starch, foaming and wetting agents, were dried at 55–80 °C. Wetting agents are surfactants (in this case FBC and SLS) added primarily to reduce the surface tension of water thereby improving the wetting of the particles by the liquid. The process was optimized and reported elsewhere [41]. After drying and burning out the

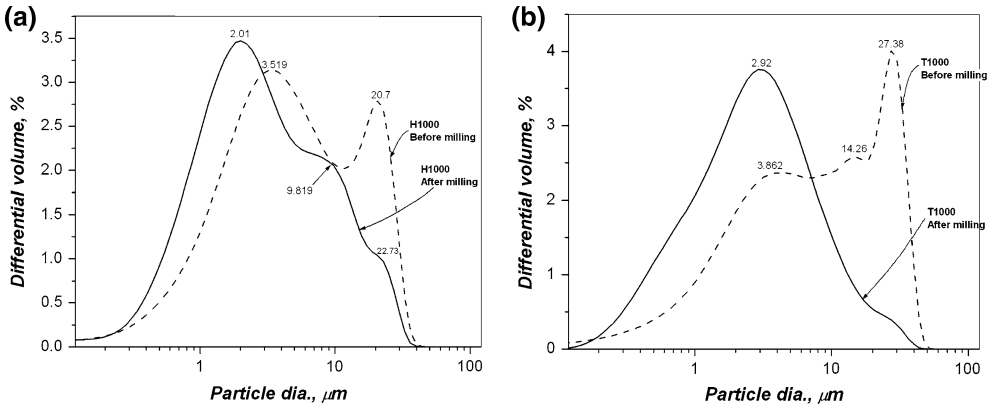

Fig. 7 Particle size distribution of the powders (calcined at 1000 °C) both before and after milling used for starch consolidation work: **a** for HAp and **b** for β-TCP

Table 3 Physical properties of porous scaffolds used for subsequent fabrication of drug delivery system

Sample	Bulk density, g/c.c.	Apparent porosity, %	Closed porosity, %	Compressive strength, MPa
H1250	0.961	67.32	2.33	30.2
T1200	1.333	55.74	2.16	66.3

organic component, the resulting green ceramic bodies were sintered at 1250° and 1200° respectively for HAp and TCP body following the schedule given in Fig. 1.

Physical parameters such as percent open porosity, closed porosity, bulk density of the samples fired at their sintering temperatures measured by Archimedes' water displacement method and compressive strength of the samples were given in Table 3.

To avoid excessive shrinkage during densification slurries containing high volume fraction of particles is desirable. Accordingly, slurries with a 45 vol% solids were used in the present investigation. For casting porous layers, the same slurry with added starch, foaming and wetting agents, were dried at 55–80 °C. At this stage, when the starch granules swell, it can be assumed that the surrounding particles (matrix) are compressed by the draining of water, forcing the particles closer to each other and, eventually, causing a flocculation process, which may assist the consolidation of the entire particulate suspension into a rigid body. At the same time the opening up of the starch granules gives an adhesion to the ceramic matrix which further contributes to the rigidity of the consolidated body. Wetting agents are surfactants (in this case FBC and SLS) added primarily to reduce the surface tension of water thereby improving the wetting of the particles by the liquid. The process was optimized and reported elsewhere. After drying and burning out the organic component, the resulting green ceramic bodies were sintered at 1250° and 1200° respectively for HAp and TCP body following the schedule given in Fig. 1.

SEM microstructures of the porous body fabricated using HAp and TCP powders are presented in Figs. 8 and 9. More than 250 linear measurements were taken from each micrograph and converted to their actual dimension from the corresponding tag of each microstructure. Histograms thus obtained were plotted as function of pore size ranges and are given in Fig. 10a and b for HAp and β-TCP respectively. Spherical morphology together with highly interconnected (>50 μm) pores were observed in both the microstructures. Spherical nature was due to the structure of the foam in the green state.

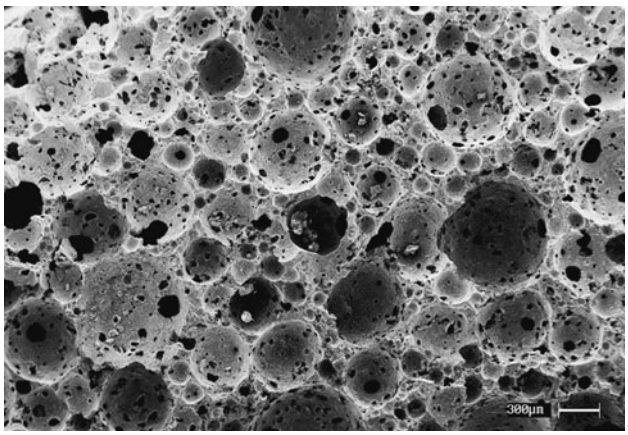

Fig. 8 SEM microstructures of porous HAp scaffold

It can be observed that over 90% of the total porosity consists of open and interconnected pores. This means that the fraction of closed pores is relatively modest if one considers that foaming methods tend to form essentially closed porosity [42]. These results suggest that the pores

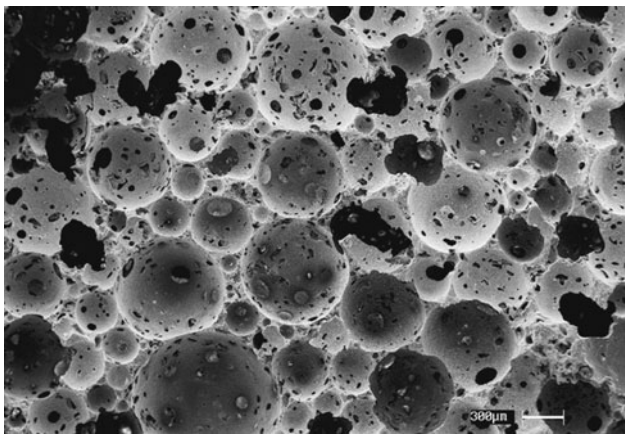

Fig. 9 SEM microstructures of porous β-TCP scaffold

left by the burning out of starch granules enhance pore interconnectivity. This also proves the suitability of combining the foaming method with the starch consolidation method to achieve the desired goals in terms of porous microstructure. However, pore size and pore interconnectivity also increases with amount of foaming agent. Porous solids can be divided into two major class according to Gibson and Ashby, viz. foams and honeycombs [43]. Irrespective of the structure of pore high degree of porosity is always desirable to accommodate the mass transfer as well as tissue development with low volume fraction of scaffold. Macropores (>50 μm) in an appropriate scale influence tissue function while micropores (<50 μm) influence the cell function (for example, cell attachment) as mammalian cells are typically of 10–20 μm in size. Pore interconnectivity is another very important factor often overlooked before scaffold design [44–46]. Interconnected pores influence more critically than pore size alone. It should be suitably large to support cell migration and proliferation in the initial stages and then ECM infiltration of desired tissue. It is desirable that scaffolds for tissue engineering and drug delivery should have 100% interconnecting pore volume which ensure maximum diffusion and exchange of nutrients (e.g. oxygen) and excretion of waste throughout the entire scaffold pore volume. The scaffold prepared for this investigation is almost ideal from the above point of views.

3.2.1 *Characterization of drug and chitosan loaded samples*

Figures 11 I and II show the microstructure of chitosan and drug coated porous HAp scaffolds. Both crystalline microstructure of HAp and its closest approximated drug at the interface infused into the pores could be seen. Cracks were also visible at the drug surface. The interface could not be distinguishable. Line scan of EDAX was performed at the points from A to D of Fig. 11 I to check the compositional variation across the interface. Corresponding graphs obtained after EDAX scan are given along with. At point A, there were abundance of the elements like S (sulphur), Na (sodium), etc. characteristics of the drugs, which were almost absent when the EDAX was taken at points B and C. These points corresponded the material (HAp in this case) with presence of peaks like Ca (calcium), P (phosphorus) and O (oxygen). H (hydrogen) could not be estimated by EDAX analysis. D was pointing towards the interface between the drug and the material, where elements corresponding the calcium phosphate and drug were present simultaneously. The presence of N (nitrogen) and C (carbon) peaks were from the mixed up chitosan in the drug. Chitosan and drug did not chemically react as evidenced by the UV–Vis spectroscopy measurements for the composite drug (ceftriaxone and sulbactum) and drug-chitosan mixture. Respective peaks for ceftriaxone and sulbactum were present even after this mixing process and pictorially represented in Fig. 12.

Figures 13 show the typical SEM microstructure of chitosan and drug coated porous β-TCP scaffolds. The drug was continuously adhered on the β-TCP pore surface. Cracks on the drug/chitosan composite surface layer are also visible. There was no interfacial gap existed.

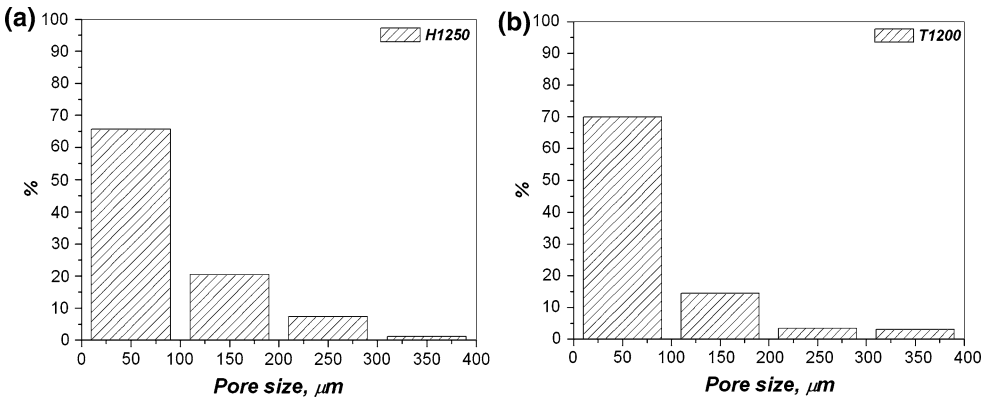

Fig. 10 Pore size distribution calculated by analyzing SEM microstructures of **a** HAp given in Fig. 8 and **b** β-TCP given in Fig. 9

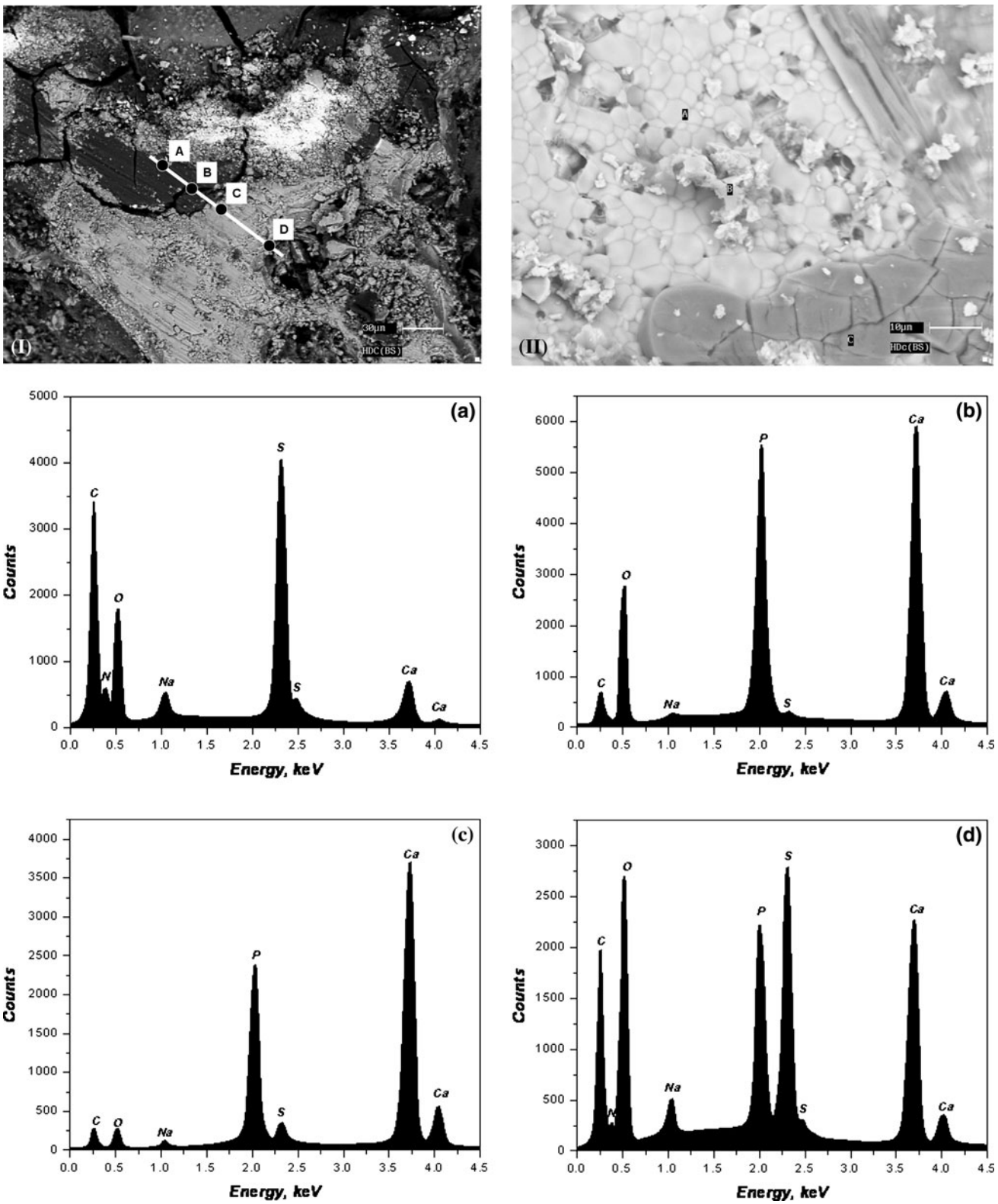

Fig. 11 I and II: SEM micrographs of chitosan and drug coated porous HAp scaffolds. EDAX were taken at the points from A–D of Fig. 11 I and are given beneath

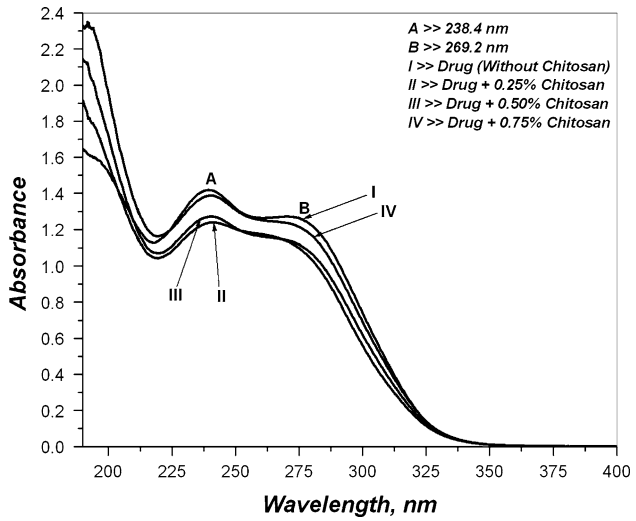

Fig. 12 UV–Vis Spectrophotometer of the samples to show the effect of chitosan on the composite drug. A and B are the characteristic peaks for ceftriaxone and sulbactum sodium, I, II, III and IV are the variation of chitosan concentration

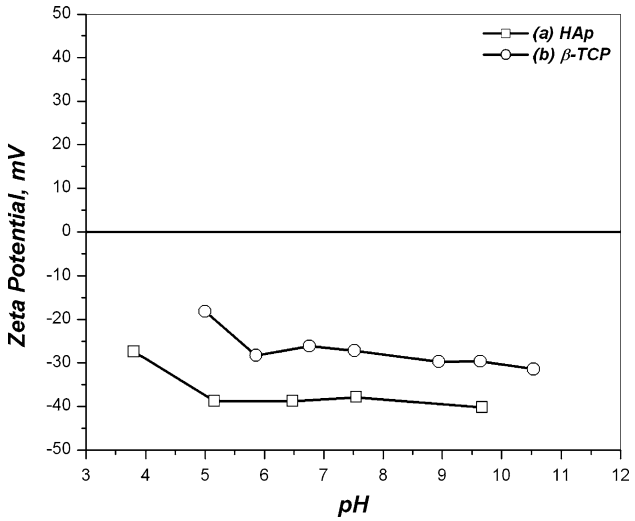

Fig. 14 Variation of surface charge in terms of zeta potential for the powders calcined at 1250 and 1200 °C for **a** HAp and **b** β-TCP respectively with respect to pH

Qualitative EDAX compositional variations were recorded from point A to B (line scan) on the microstructure and were given in the same figure. Variation of the elements like C, N, O, Na, P, S and Ca were recorded. There were maximum amounts of Ca and P and moderate O present in between points A and B, resembled the presence of calcium phosphate phase (β-TCP in this case) that could be seen as whiter part in the microstructure. Points A and B are drug-rich as S, Na and C were detected at these two extreme points when EDAX scans were taken. Nitrogen (N) was present throughout A–B as chitosan formed a film onto the pore surface throughout the microstructure.

Chitosan is a natural polymer which has many interesting physicochemical properties viz. it is polycationic, has reactive OH and NH_2 groups and biological properties viz. it is bioactive, biocompatible and biodegradable, recently known to have insecticidal and fungicidal activity too [47]. The unique chemical structure of chitosan, consisting of a linear polyelectrolyte chains with a high charge density having reactive hydroxyl and amino groups, confers them very good flocculent properties, which adhere to the negatively charged surfaces with biocompatible, nontoxic, biodegradable and fungicidal activities. The close apposition of this drug + chitosan combination to the calcium phosphates can be understood considering the predominant negative surface charge of these calcium phosphates in aqueous media within broad pH range. Figure 14 plots the zeta potential for HAp and TCP powders fired at 1250 and 1200 °C, respectively, as function of pH.

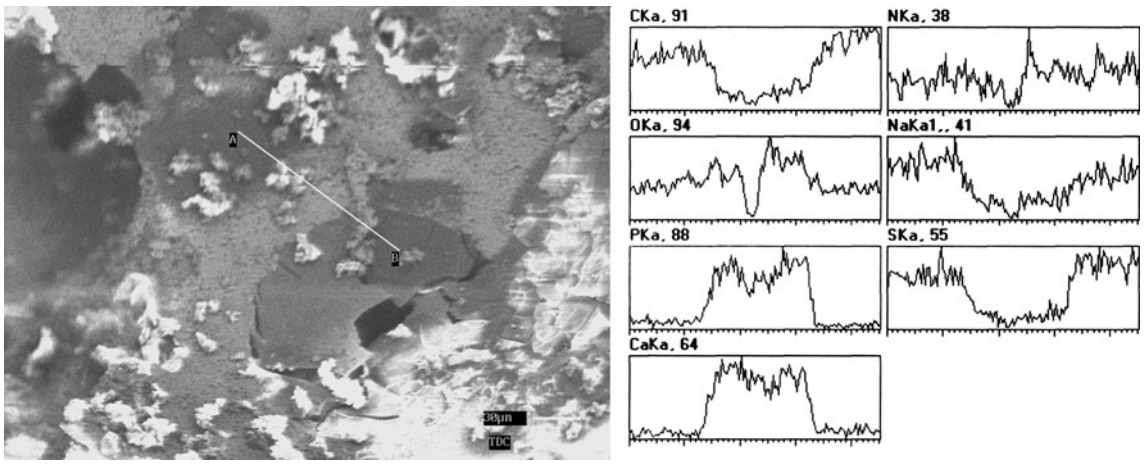

Fig. 13 SEM micrographs of chitosan and drug coated porous β-TCP scaffolds. EDAX line scans were taken from points A–B. Compositional variation were considered for the elements like C, N, O, Na, P, S and Ca

It was found that both these powders showed anionic nature in aqueous suspension and HAp had more surface potential in all the pH range than the corresponding β-TCP in water. This indicates that chitosan might have stronger affinity to HAp than to β-TCP. Zeta potential was particularly used for assessment of deflocculation characteristics while fabricating the porous calcium phosphate scaffold. However, this parameter was never discussed for its effect on drug attachment to the pore surface of HAp/TCP scaffold. In our study, HAp surface in aqueous media at the physiological pH (7.4), had a moderately higher negative zeta potential than TCP ($\sim$37.9 vs. 27.2 mV) which was another factor responsible for better drug adhesion characteristics as evidenced from SEM photographs. Recently negative surface charges of HAp have been reported to influence apatite nucleation, rapid cell attachment and faster tissue ingrowth [48].

Many authors proposed the use of bilayered osteochondral constructs for the improved regeneration of cartilage defects [49, 50]. The idea was to develop a single 3D porous structure that combines a mechanical support resembling the subchondral bone (bone-like layer) and to provide a chondrogenic support in the top for the repairing of cartilage (cartilage-like layer). Based on this approach, development of bilayered scaffolds combining HAp and CS layers are justified. Further, tissue engineering aims at developing tailored biomaterials which can also releasing capability of chemicals, drugs and growth factors at controlled kinetics [51]. According to Palazzo et al, a hoped goal is to produce a bone filling biomaterial with the appropriate architectural and mechanical properties realizing osteoconduction and osteoinduction through a controlled release of biological active molecules at the living tissue graft interface [52]. Implantable delivery systems, with sustained drug release likewise may be an alternative therapy for bone infection viz. chronic osteomyelitis. This implant permits an increase of the dose at the site of infection, decreasing the frequency or eliminating systemic side effects.

Chronic osteomyelitis in adults is very common in adults. Over time, a variety of conditions have been used to describe chronicity of osteomyelitis, viz., presence of draining sinus, prolonged disease duration and disease resistant to a course of antimicrobial therapy [53]. Drainage and debridement with long-term specific antimicrobial therapy are essential. The therapy include 4–6 weeks course of high-dose parenteral treatment directed at organisms. The regime was selected because that much time is required for bone to revascularize. A variety of β-lactam antimicrobials were successful. These are often given parenterally in high doses for $\sim$2 weeks and then may be given orally for a subsequent 3–4 week period. In this study, the said drug combination at a concentration of 500 mg/ml was employed for loading drugs in the porous scaffolds, as it was the concentration nearing saturation in the employed solvent at laboratory conditions [54].

3.3 In vitro drug elution study

Release profiles of the drugs ceftriaxone sodium and sulbactum sodium in PBS are plotted separately for HAp and β-TCP in Figs. 15 and 16 respectively. The observed release period was taken from 4 to 42 days (the maximum duration period studied). In general there was a burst release observed from all the samples followed by a much reduced release profile. It was observed that chitosan coating had a significant effect on suppressing the burst effect and prolonging the release period. When comparing the release of different drugs from biomaterials, factors such as size, solubility and binding capacity should play a crucial role

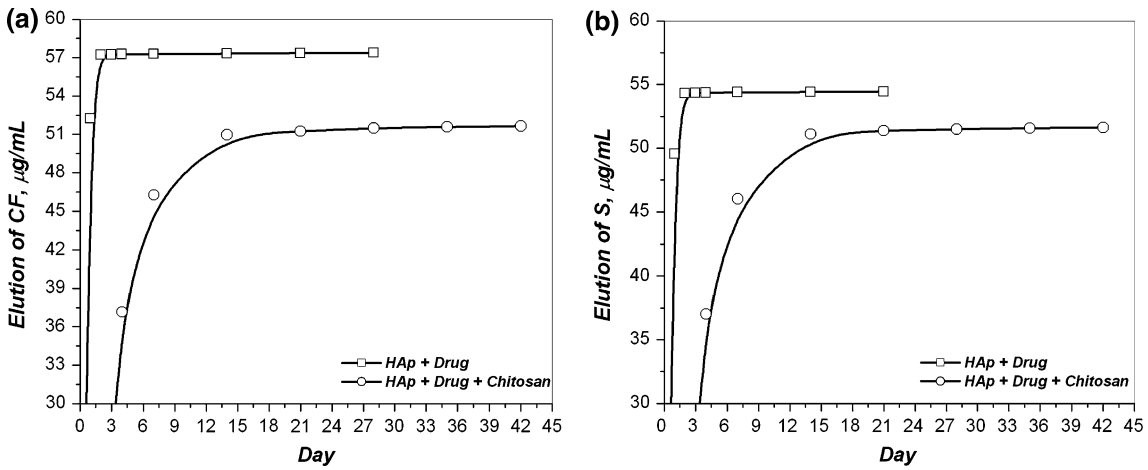

Fig. 15 In vitro drug elution kinetics for **a** ceftriaxone sodium and **b** sulbactum sodium in PBS for HAp scaffolds (Gr. I and III)

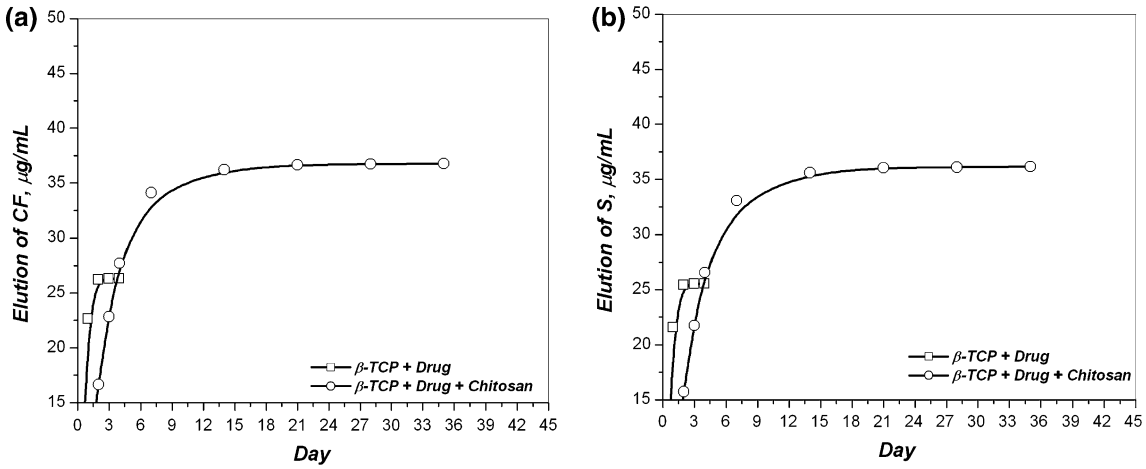

Fig. 16 In vitro drug elution kinetics for **a** ceftriaxone sodium and **b** sulbactum sodium in PBS for β-TCP scaffolds (Gr. II and IV)

[55, 56]. Obviously, the smaller molecules with greater mobility will easily pass through the pores. Accordingly, it is expected that sulbactam being a smaller molecule with molecular mass of 255.22 (in comparison to the molecular mass of 661.6 of ceftriaxone) would release faster. But, we observed that release of both the drugs were almost similar indicating higher bonding strength of sulbactam with the scaffold material. However, the release of both the drugs from HAp blocks were much slower than from β-TCP. Faster dissolution of β-TCP along with lower binding strength is responsible for these phenomena [57]. The –COOH groups present in the drug molecule are primarily responsible for binding with ceramic biomaterials and the intensity of binding increases with the number of available carboxyl groups [58]. Since both the studied drugs have just one carboxyl group available, it is evident from the release kinetics of drugs that they are materials specific.

The effect of chitosan coat on drug release could also be observed from the Figs. 15 and 16. Chitosan is positively charged and hence interacts with negatively charged polymer macromolecules and polyanions in aqueous environment [59]. Its low solubility at physiological pH 7.4 together with its affinity for water absorption and swelling behaviour retard drug release. In all samples the burst release was greatly reduced (e.g. from about 52 μg/ml to 37 μg/ml of ceftriaxone in HAp samples) and the duration of release prolonged (e.g. from 4 to 35 days in β-TCP samples). As the chitosan coat swells it forms a diffusional barrier for the drug to leach into the dissolution medium. But in the case of drug loaded β-TCP samples the total amount of drug release is more than the release from uncoated TCP. This could be due to the affinity of binding between the drugs and β-TCP and the method of chitosan coating. The negative pressure applied along with the weakly acidic chitosan solution bubbled through the pores of sample could have detached the drug from the surface and allowed it to interact with the polymer forming a drug-polymer composite. However further studies on the chemistry of interaction between drugs biomaterials and polymers are needed for a better justification.

The flux of a substance across a porous layer is connected to two main parameters: its solubility in the interested solution (in this case the physiological liquids) and the possible physical or chemical bonds formed by its molecules with the walls of the pores of the delivery device. The porous layer, which comes into contact with the living tissues, must have a chemical and physical nature biocompatible with the surrounding living tissues. Moreover, its microstructure must be compatible with its target, which is the functional activity of flux regulation of delivering; in particular its pore size distribution must ensure a continuous controlled release over time for a functional use of the dispenser.

Irrespective of benefits claimed, limitations of this delivery system, as in case of any unforeseen, unpredictable, unfortunate, rare event demanding the removal of the delivery system it would not be possible without the support of a trained medical team, as with any implantable drug delivery system. Besides, local irritation may occur due to direct exposure with bone.

4 Conclusions

A bone substitute, which also behaved as a drug delivery system, based on porous scaffolds of HAp and β-TCP, were successfully developed in the present work by applying together the techniques of starch consolidation and foaming method. Results of microstructure and pore size distribution confirmed the high percentage and high

interconnection of the porous scaffolds developed by this method. Among the materials studied, HAp exhibited better drug release profile than β-TCP when CFS was used alone; due to the higher affinity of the respective functional groups as supported by the results of surface potential. However, bilayered coating of chitosan with CFS provided prolonged release pattern for more than five weeks irrespective of the scaffold material, a period that is considered to be sufficient for local drug delivery to combat osteomyelitis. The study of SEM along with EDAX taken on the drug-chitosan bilayerd scaffold showed closest apposition of this combination to the calcium phosphate surface. This study leads to conclude that the ability of porous drug delivery systems developed by starch consolidation along with foaming method to release drug is highly influenced by the selection of carrier material. However, this restriction could be relaxed by forming a bilayered scaffold.

Acknowledgments The authors wish to express their sincere thanks to Department of Science and Technology, India and Fundação para a Ciência e a Tecnologia, Portugal for funding this work and the Director, CGCRI, India and CICECO, University of Aveiro, Portugal for their support. All the personnel related to the characterization of the materials are sincerely acknowledged.

References

1. Soundrapandian C, Datta S, Sa B. Drug-eluting implants for osteomyelitis. Crit Rev Ther Drug Carrier Syst. 2007;24(6):493–545.
2. Soundrapandian C, Sa B, Datta S. Organic-inorganic composites for bone drug delivery. AAPS PharmSciTech. 2009;10(4):1158–71.
3. Chen L, Wang H, Wang J, Chen M, Shang L. Ofloxacin-delivery system of a polyanhydride and polylactide blend used in the treatment of bone infection. J Biomed Mater Res B Appl Biomater. 2007;83(2):589–95.
4. Efstathopoulos N, Giamarellos-Bourboulis E, Kanellakopoulou K, Lazarettos I, Giannoudis P, Frangia K, et al. Treatment of experimental osteomyelitis by methicillin resistant staphylococcus aureus with bone cement system releasing grepafloxacin. Injury. 2008;39(12):1384–90.
5. Liu-Snyder P, Webster TJ. Developing a new generation of bone cements with nanotechnology. Curr Nanosci. 2008;4(1):111–8.
6. Anagnostakos K, Hitzler P, Pape D, Kohn D, Kelm J. Persistence of bacterial growth on antibiotic-loaded beads: Is it actually a problem? Acta Orthop. 2008;79(2):302–7.
7. Nandi SK, Kundu B, Ghosh SK, De DK, Basu D. Efficacy of nano-hydroxyapatite prepared by an aqueous solution combustion technique in healing bone defects of goat. J Vet Sci. 2008;9(2):183–91.
8. Nandi SK, Ghosh SK, Kundu B, De DK, Basu D. Evaluation of new porous β-tri-calcium phosphate ceramic as bone substitute in goat model. Small Ruminant Res. 2008;75(2–3):144–53.
9. Ghosh SK, Nandi SK, Kundu B, Datta S, De DK, Roy SK, et al. In vivo response of porous hydroxyapatite and beta-tricalcium phosphate prepared by aqueous solution combustion method and comparison with bioglass scaffolds. J Biomed Mater Res B Appl Biomater. 2008;86(1):217–27.
10. Nandi SK, Kundu B, Ghosh SK, Mandal TK, Datta S, De DK, et al. Cefuroxime-impregnated calcium phosphates as an implantable delivery system in experimental osteomyelitis. Ceram Int. 2009;35(4):1367–76.
11. Nandi SK, Mukherjee P, Roy S, Kundu B, De DK, Basu D. Local antibiotic delivery systems for the treatment of osteomyelitis–a review. Mater Sci Engg C. 2009;29(8):2478–85.
12. Nandi SK, Kundu B, Mukherjee P, Mandal TK, Datta S, De DK, et al. In vitro and in vivo release of cefuroxime axetil from bioactive glass as an implantable delivery system in experimental osteomyelitis. Ceram Int. 2009;35(8):3207–16.
13. Klawitter JJ, Hulbert SF. Application of porous ceramics for the attachment of load bearing internal orthopaedic application. J Biomed Mater Res Symposium No 2. 1971;Part 1:161-229.
14. de Groot K, Klein CPAT, Wolke JGC, de Blieck-Hogervorst JMA. Chemistry of calcium phosphate bioceramics. In: Yamamuro T, Hench LL, Wilson J, editors. Handbook of bioactive ceramics. Vol. 2: Calcium phosphate and hydroxylapatite ceramics. Boca Raton: CRC Press; 1990. p. 3–16.
15. White EW, Weber JN, Roy DM, Owen EL, Chiroff RT, White RA. Replamineform porous biomaterials for hard tissue implant applications. J Biomed Mater Res. 1975;9(4):23–7.
16. Hulbert SF, Morrison SJ, Klawitter JJ. Tissue reaction to three ceramics of porous and non-porous structures. J Biomed Mater Res. 1972;6(5):347–74.
17. Sopyan I, Mel M, Ramesh S, K.A. K. Porous hydroxyapatite for artificial bone applications. Sci Tech Adv Mater. 2007;8:116–23.
18. Lyckfeldt O, Ferreira JMF. Processing of porous ceramics by 'starch consolidation'. J Eur Ceram Soc. 1998;18(2):131–40.
19. Rutenberg M. Starch and its modifications. Handbook of water-soluble gums and resins. New York: McGraw Hill; 1979.
20. Shrivastava SM, Saurabh S, Rai D, Dwivedi VK, Chaudhary M. In vitro microbial efficacy of sulbactomax: A novel fixed dose combination of ceftriaxone sulbactam and ceftriaxone alone. Curr Drug Ther. 2009;4(1):73–7.
21. Zhao F, Grayson WL, Ma T, Bunnell B, Lu WW. Effects of hydroxyapatite in 3-d chitosan-gelatin polymer network on human mesenchymal stem cell construct development. Biomaterials. 2006;27(9):1859–67.
22. Zhang L, Ao Q, Wang A, Lu G, Kong L, Gong Y, et al. A sandwich tubular scaffold derived from chitosan for blood vessel tissue engineering. J Biomed Mater Res A. 2006;77(2):277–84.
23. Ao Q, Wang A, Cao W, Zhang L, Kong L, He Q, et al. Manufacture of multimicrotubule chitosan nerve conduits with novel molds and characterization in vitro. J Biomed Mater Res A. 2006;77(1):11–8.
24. Kong L, Gao Y, Cao W, Gong Y, Zhao N, Zhang X. Preparation and characterization of nano-hydroxyapatite/chitosan composite scaffolds. J Biomed Mater Res A. 2005;75(2):275–82.
25. Kundu B, Sarkar R, Banerjee G, Panda C, Basu D, inventors; Central Glass and Ceramic Research Institute IFGL Bioceramics Limited, assignee. An improved process for the synthesis of pure beta-tri-calcium phosphate (β-tcp) useful for biomedical application (applied). India 2009.
26. Kundu B, Sinha MK, Mitra MK, Basu D. Fabrication and characterization of porous hydroxyapatite ocular implant followed by an in vivo study in dogs. Bull Mater Sci. 2004;27(2):133–40.
27. Rodriguez-Lorenzo LM, Vallet-Regi M, Ferreira JM. Colloidal processing of hydroxyapatite. Biomaterials. 2001;22(13):1847–52.
28. Lemos AF, Santos JD, Ferreira JMF. New method for the incorporation of soluble bioactive glasses to reinforce porous ha structures. Key Engg Mater. 2003;254–256:1033–6.
29. ASTM Standard C773-88. Standard test method for compressive (crushing) strength of fired whiteware materials. West

Conshohocken, PA: ASTM International; 2006. doi:10.1520/C0773-88R06.
30. Klug HP, Alexander LE. X-ray diffraction procedures: For polycrystalline and amorphous materials. 2 ed. ed. Weinheim: Wiley-VCH; 1974.
31. Cullity BD, Stock SR. Elements of x-ray diffraction. 2 ed. ed. New Jersey: Prentice Hall; 2001.
32. Landi E, Tampieri A, Celotti G, Sprio S. Densification behaviour and mechanisms of synthetic hydroxyapatites. J Eur Ceram Soc. 2000;20(14–15):2377–87.
33. LeGeros RZ. Calcium phosphates in oral biology and medicine. Monogr Oral Sci. 1991;15:1–201.
34. Silva CC, Pinheiro AG, Miranda MAR, Goes JC, Sombra ASB. Structural properties of hydroxyapatite obtained by mechanosynthesis. Solid State Sci. 2003;5(4):553–8.
35. Mostafa NY. Characterization, thermal stability and sintering of hydroxyapatite powders prepared by different routes. Mater Chem Phys. 2005;94(2–3):333–41.
36. Yoshimura M, Suda H, Okamoto K, Ioku K. Hydrothermal synthesis of biocompatible whiskers. J Mater Sci. 1994;29(13):3399–402.
37. Nelson DG, Featherstone JD. Preparation, analysis, and characterization of carbonated apatites. Calcif Tissue Int. 1982;34(Suppl 2):S69–81.
38. Kutty TRN. Assignments of some bands in the infrared spectrum of b-tricalcium phosphate. Ind J Chem. 1970;8(7):655–7.
39. Jinawath S, Polchai D, Yoshimura M. Low-temperature, hydrothermal transformation of aragonite to hydroxyapatite. Mater Sci Engg C. 2002;22(1):35–9.
40. Rahaman MN. Ceramic processing and sintering. 2 ed. ed. New York: Marcel Dekker; 2003.
41. Lemos AF, Ferreira JMF. Combining foaming and starch consolidation methods to develop macroporous ha implants. Key Engg Mater. 2004;254–256:1041–4.
42. Minnear WP. Processing of foamed ceramics. Ceramic transactions, forming science and technology for ceramics. Westemille, Ohio: The American Ceramic Society; 1992.
43. Gibson LJ, Ashby MF. Cellular solids: Structure and properties. 2 ed. ed. Cambridge: Cambridge University Press; 1997.
44. Kuhne JH, Bartl R, Frisch B, Hammer C, Jansson V, Zimmer M. Bone formation in coralline hydroxyapatite. Effects of pore size studied in rabbits. Acta Orthop Scand. 1994;65(3):246–52.
45. Eggli PS, Muller W, Schenk RK. Porous hydroxyapatite and tricalcium phosphate cylinders with two different pore size ranges implanted in the cancellous bone of rabbits. A comparative histomorphometric and histologic study of bony ingrowth and implant substitution. Clin Orthop Relat Res. 1988;232:127–38.
46. Holmes R, Mooney V, Bucholz R, Tencer A. A coralline hydroxyapatite bone graft substitute. Preliminary report. Clin Orthop Relat Res. 1984;188:252–62.
47. Zhang M, Tan T, Yuan H, Rui C. Insecticidal and fungicidal activities of chitosan and oligo-chitosan. J Bioactive Compat Polym. 2003;18(5):391–400.
48. Bodhak S, Bose S, Bandyopadhyay A. Role of surface charge and wettability on early stage mineralization and bone cell-materials interactions of polarized hydroxyapatite. Acta Biomater. 2009;5(6):2178–88.
49. Lima EG, Mauck RL, Han SH, Park S, Ng KW, Ateshian GA, et al. Functional tissue engineering of chondral and osteochondral constructs. Biorheology. 2004;41(3–4):577–90.
50. Schaefer D, Martin I, Shastri P, Padera RF, Langer R, Freed LE, et al. In vitro generation of osteochondral composites. Biomaterials. 2000;21(24):2599–606.
51. Mahoney MJ, Saltzman WM. Transplantation of brain cells assembled around a programmable synthetic microenvironment. Nat Biotechnol. 2001;19(10):934–9.
52. Palazzo B, Sidoti MC, Roveri N, Tampieri A, Sandri M, Bertolazzi L, et al. Controlled drug delivery from porous hydroxyapatite grafts: An experimental and theoretical approach. Mater Sci Engg C. 2005;25(2):207–13.
53. Rissing JP. Antimicrobial therapy for chronic osteomyelitis in adults: Role of the quinolones. Clin Infect Dis. 1997;25(6):1327–33.
54. Bush K. Beta-lactamase inhibitors from laboratory to clinic. Clin Microbiol Rev. 1988;1(1):109–23.
55. Lebugle A, Rodrigues A, Bonnevialle P, Voigt JJ, Canal P, Rodriguez F. Study of implantable calcium phosphate systems for the slow release of methotrexate. Biomaterials. 2002;23(16):3517–22.
56. Burgos AE, Belchior JC, Sinisterra RD. Controlled release of rhodium (ii) carboxylates and their association complexes with cyclodextrins from hydroxyapatite matrix. Biomaterials. 2002;23(12):2519–26.
57. LeGeros RZ, Bautista C, LeGeros JP, Vijaraghavan TV, Retino M. Comparative properties of bioactive bone graft materials. Bioceramics. London: Pergamon Press; 1995.
58. Stigter M, Bezemer J, de Groot K, Layrolle P. Incorporation of different antibiotics into carbonated hydroxyapatite coatings on titanium implants, release and antibiotic efficacy. J Control Release. 2004;99(1):127–37.
59. Prabaharan M. Chitosan derivatives as promising materials for controlled drug delivery. J Biomater Appl. 2008;23(1):5–36.